Electron beams and loss cones in the auroral regions of Jupiter

F. Allegrini, F. Bagenal, S. Bolton, J. Connerney, G. Clark, R. W. Ebert, T. K. Kim, W. S. Kurth, S. Levin, P. Louarn, et al.

AGU PUBLICATIONS

Geophysical Research Letters

RESEARCH LETTER
10.1002/2017GL073180

Special Section:
Early Results: Juno at Jupiter

Electron beams and loss cones in the auroral regions of Jupiter

F. Allegrini[1,2], F. Bagenal[3], S. Bolton[1], J. Connerney[4], G. Clark[5], R. W. Ebert[1], T. K. Kim[1,2], W. S. Kurth[6], S. Levin[7], P. Louarn[8], B. Mauk[5], D. J. McComas[1,9,10], C. Pollock[11], D. Ranquist[3], M. Reno[12], J. R. Szalay[1], M. F. Thomsen[13], P. Valek[1,2], S. Weidner[10], R. J. Wilson[3], and J. L. Zink[1,2]

[1]Southwest Research Institute, San Antonio, Texas, USA, [2]Department of Physics and Astronomy, University of Texas at San Antonio, San Antonio, Texas, USA, [3]Laboratory for Atmospheric and Space Physics, University of Colorado Boulder, Boulder, Colorado, USA, [4]Goddard Space Flight Center, Greenbelt, Maryland, USA, [5]The Johns Hopkins University Applied Physics Laboratory, Laurel, Maryland, USA, [6]Department of Physics and Astronomy, University of Iowa, Iowa City, Iowa, USA, [7]Jet Propulsion Laboratory, Pasadena, California, USA, [8]Institut de Recherche en Astrophysique et Planétologie, Toulouse, France, [9]Department of Astrophysical Sciences, Princeton University, Princeton, New Jersey, USA, [10]Office of the VP for Princeton Plasma Physics Laboratory, Princeton University, Princeton, New Jersey, USA, [11]Denali Scientific, Healy, Alaska, USA, [12]Austin Mission Consulting, Austin, Texas, USA, [13]Planetary Science Institute, Tucson, Arizona, USA

Abstract We report on the first observations of 100 eV to 100 keV electrons over the auroral regions of Jupiter by the Jovian Auroral Distributions Experiment (JADE) on board the Juno mission. The focus is on the regions that were magnetically connected to the main auroral oval. Amongst the most remarkable features, JADE observed electron beams, mostly upward going but also some downward going in the south, at latitudes from ~69° to 72° and ~ −66° to −70° corresponding to M shells ("M" for magnetic) from ~18 to 54 and ~28 to 61, respectively. The beams were replaced by upward loss cones at lower latitudes. There was no evidence of strongly accelerated downward electrons analogous to the auroral "inverted Vs" at Earth. Rather, the presence of upward loss cones suggests a diffuse aurora process. The energy spectra resemble tails of distributions or power laws (suggestive of a stochastic acceleration process) but can also have some clear enhancements or even peaks generally between 1 and 10 keV. Electron intensities change on timescales of a second or less at times implying that auroral structures can be of the order of a few tens of kilometers.

Key Points:
- First 100 eV to 100 keV electron measurements in the auroral regions of Jupiter
- Upward and downward electron beams observed in the polar regions and on field lines connected to the middle plasma sheet
- Upward loss cone on the field lines connected to the inner plasma sheet suggesting a diffuse aurora process

Correspondence to:
F. Allegrini,
fallegrini@swri.edu

Citation:
Allegrini, F., et al. (2017), Electron beams and loss cones in the auroral regions of Jupiter, *Geophys. Res. Lett.*, *44*, 7131–7139, doi:10.1002/2017GL073180.

Received 20 FEB 2017
Accepted 18 APR 2017
Published online 27 JUL 2017

1. Introduction

Juno flew over Jupiter's polar regions on 27 August 2016 providing the first plasma measurements at low altitude in the auroral regions of Jupiter. Preliminary results from Juno's magnetospheric science are summarized in *Connerney et al.* [2017a]. Juno includes a comprehensive suite of instruments to characterize Jupiter's magnetosphere [*Bagenal et al.*, 2014]: MAG is a magnetometer [*Connerney*, 2017b], the Jovian Auroral Distributions Experiment (JADE) is an ion and electron plasma instrument [*McComas et al.*, 2013], Jupiter Energetic Particle Detector Instrument (JEDI) is an energetic ion and electron instrument [*Mauk et al.*, 2014], Waves is a plasma waves instrument, UVS is a UV spectrometer [*Gladstone et al.*, 2014], and Jovian Infrared Auroral Mapper (JIRAM) is an infrared imager [*Adriani et al.*, 2014].

Before Juno's first primary science orbit, JADE measured solar wind ions and magnetospheric ions and electrons with key structures identified in *McComas et al.* [2017], evidence for magnetic reconnection in *Ebert et al.* [2017], a very large hot flow anomaly in the solar wind [*Valek et al.* 2017]. JADE also contributed to a study on magnetopause crossings [*Gershman et al.*, 2017]. *Szalay et al.* [2017] mapped the different regions sampled over the auroral regions to the equatorial magnetosphere for the first science orbit.

No spacecraft has sampled latitudes higher than about 20°, except for the flybys of Pioneer 11 and Ulysses, which derived electron densities from less than 0.01 to about 0.1 cm^{-3} and temperature $1–2 \cdot 10^6$ K [*Phillips et al.*, 1993]. Here we report on the first observations of 100 eV to 100 keV electrons in Jupiter's auroral regions by JADE. We first describe the JADE-Electron (JADE-E) instrument characteristics and the data used. Then, we show an overview of auroral electron measurements for this first science perijove pass. We give pitch angle distributions and energy spectra of chosen intervals in the auroral region when Juno is connected to different regions of the plasma sheet and the polar regions. In particular, we highlight observations of upward and downward electron beams and upward loss cones.

2. Data

JADE-E consists of two (originally three, but one is off due to a high-voltage component failure) identical top-hat electrostatic energy analyzers that measure electrons from ~100 eV up to ~100 keV with an energy resolution of the order of 10 to 14% at 1 s time resolution [*McComas et al*., 2013]. Each analyzer covers 120° in azimuth (Juno's spin plane) and has deflectors to track the direction of the magnetic field up to ±35° in elevation (up to 40 keV; ~ ±15° at 100 keV). The angular resolution is ~7.5° in azimuth and ~2–5.5° in elevation. The magnetic vector components are received every 2 s from MAG [*Connerney et al*., 2017b] and are propagated using the spacecraft spin rate to calculate the required deflection angle.

For this study, we used the JADE version 01 data set from PDS volume JNO-J/SW-JAD-3-CALIBRATED-V1.0 and JNO-J/SW-JAD-2-UNCALIBRATED-V1.0 at 1 s time resolution.

The JADE-E detectors are equipped with background anodes. The background anode has the same front-end electronics as the signal anodes, but a mask blocks the electrons coming from the electrostatic analyzer. The rate measured on the background anode is used to estimate the rate induced by penetrating radiation on the signal anodes. The background estimate is then subtracted from the signal. While most of the radiation-induced background has been removed from the signal with this method, there is still occasionally some residual background.

To calculate the pitch angle (PA) for each look direction, we used the onboard reported values from MAG. The precision of the PA calculation is sufficient (i.e., better than the ~7.5° angular resolution of JADE-E) for this preliminary study.

3. Results

Figures 1 and 2 give an overview of the electron measurements for the north and south crossings of the magnetic field lines connected to the main auroral oval. Figure 1a shows Juno's trajectory (thick black line) in a magnetic coordinate system (VIP4 [*Connerney et al*., 1981]) where the vertical axis is aligned with the magnetic dipole. Figure 1b shows a projection of Juno's magnetic footprint looking down on Jupiter's northern ionosphere, where the blue solid/dotted lines represent the average center and boundaries of the main auroral oval derived from Hubble Space Telescope observations [*Bonfond et al*., 2012]. The black cross is the north magnetic pole. The colored dots in Figures 1a and 1b are sized and color-coded according to electron intensities, using the color bar of Figure 1c.

Figure 1c shows the count rate versus energy spectrogram (summed over all look directions) and Figure 1d the electron PA spectrogram (summed over all energies) as a function of time. The scales at the bottom indicate the time (UTC), the magnetic latitude, the M shell (see below), the distance to Jupiter's center, the magnetic field strength calculated from the onboard received values, and the spacecraft speed. We use the terminology "M shell" (M for magnetic) as an alternative for L shell due to the fact that the equatorial crossing distances are strongly affected by the stretched field lines and deviate from the traditional dipole picture. The M shell distance mapping is derived using VIP4 + CAN [*Connerney et al*., 1981, 1998].

The period of interest is mapped to well equatorward of the average main oval in Figure 1b. While this is unexpected, there are some reasons that can explain why. First, a UVS composite image [*Bonfond et al*., 2017] accumulated just minutes before this time interval shows somewhat bright, narrow emissions well equatorward of the main oval average location, while the emissions in the main oval region are fairly dim. Second, different models map Juno's foot point differently. Third, the longitude of this pass is near a magnetic anomaly that would influence the mapping [*Grodent et al*., 2008, *Vogt et al*., 2011]. Fourth, this also corresponds to a region of diffuse emission in the duskside, which seemed to be always present in observations by Hubble Space Telescope between 1997 and 2007 [*Radioti et al*., 2009].

The vertical dashed lines in Figure 1c show boundaries as defined in *Szalay et al*. [2017], which correspond to Juno magnetically mapping to different regions in the magnetosphere. These authors used ion composition and energy spectra, as well as electron data, to define these boundaries. Here we summarize the boundaries that fall within the time range of the plot and label these regions on top of Figure 1c. Before ~12:10:13, Juno was connected to the polar region and outer magnetosphere

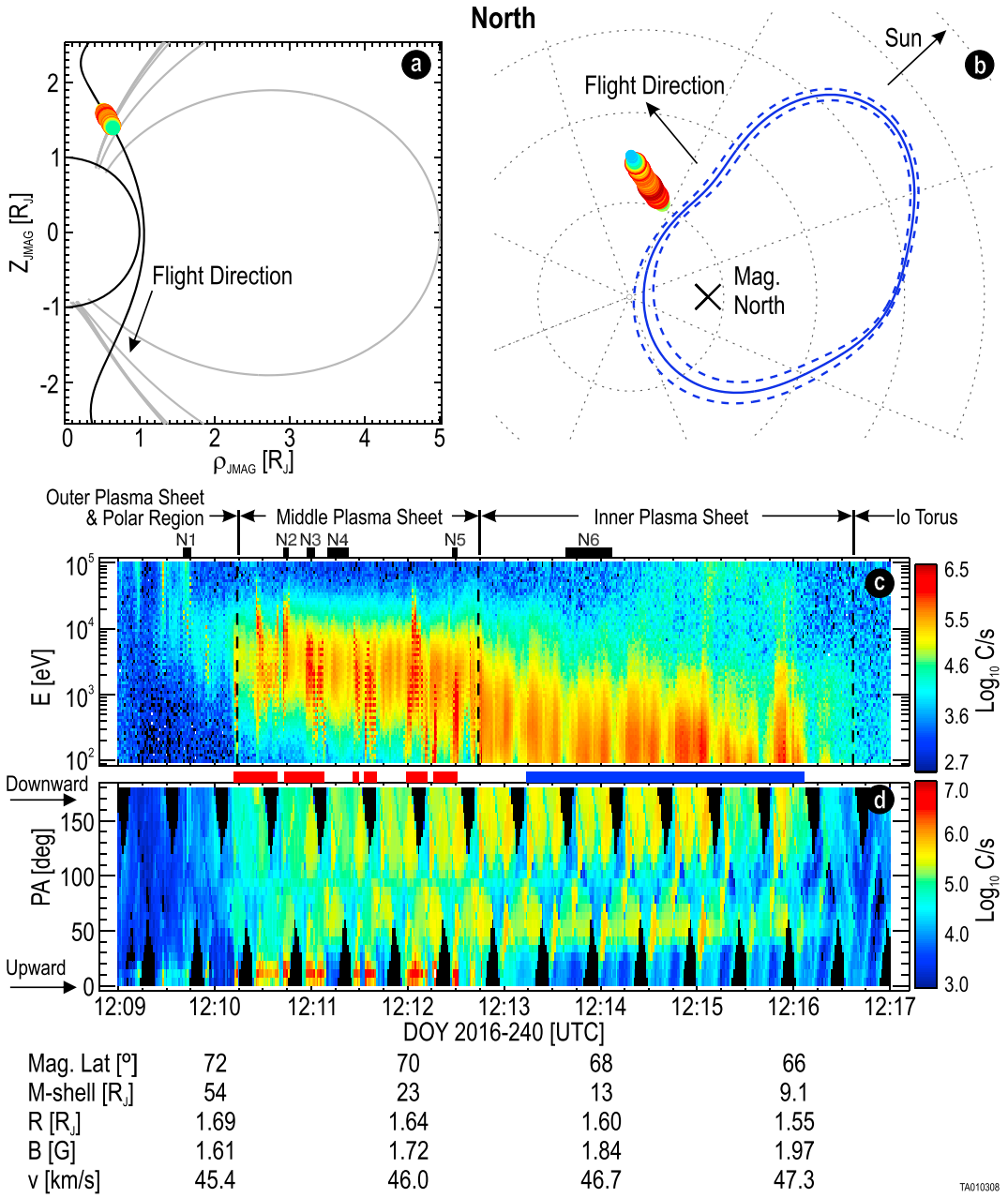

Figure 1. Overview of the north pass. (a) A projection of Juno's trajectory in a magnetic dipole reference frame. The color dots indicate the electron intensities for the interval of Figures 1c and 1d. (b) A projection of the north pole with Juno's magnetic footprint (colored dots) and the average location of the main auroral oval (blue solid and dashed lines). (c and d) The electron energy and PA spectrograms. PA = 0 corresponds to the upward direction and PA = 180° to the downward direction (toward Jupiter).

(M shell >52). Between 12:10:13 and 12:12:43, Juno was connected to the middle plasma sheet. Next, it was connected to the inner plasma sheet until about 12:16:36. And after that, Juno was connected to the Io plasma torus. We expect the main auroral oval to be around M shells 20–30 R_J where co-rotation of the plasma sheet breaks down, somewhere in the interval labeled middle plasma sheet in Figure 1c. This is slightly outside the average location of the main oval as shown in Figure 1b.

When Juno was connected to the polar region and outer plasma sheet, electrons started to appear sporadically in JADE-E's energy range with decreasing energy until their energy reached about 1–10 keV. Electrons at energies higher than ~10 keV were mostly field aligned and going in the upward direction (PA ~ 0). At

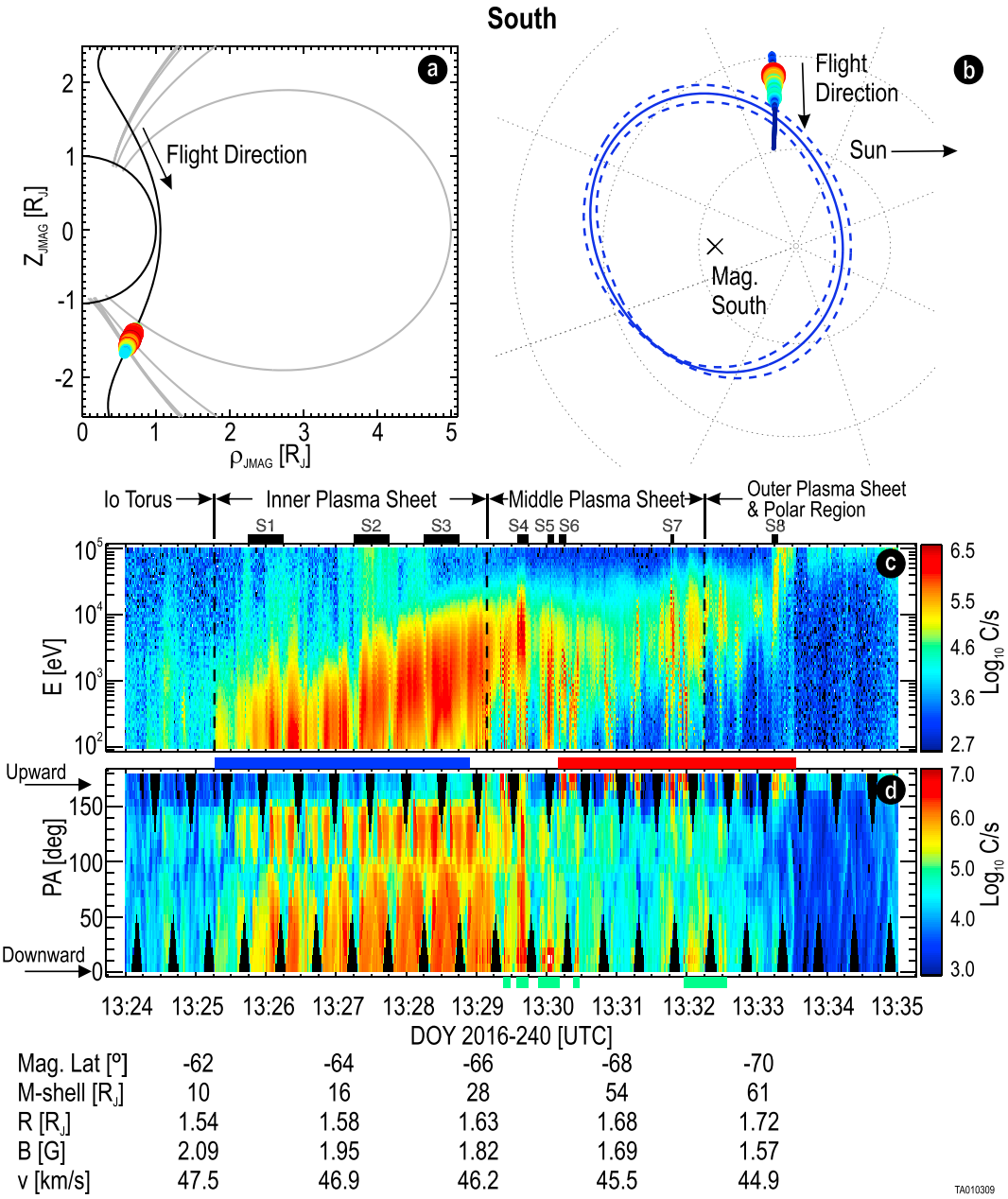

Mag. Lat [°]	-62	-64	-66	-68	-70
M-shell [R_J]	10	16	28	54	61
R [R_J]	1.54	1.58	1.63	1.68	1.72
B [G]	2.09	1.95	1.82	1.69	1.57
v [km/s]	47.5	46.9	46.2	45.5	44.9

Figure 2. Overview of the south pass. This figure is similar to Figure 1 with the notable difference that PA = 0 corresponds to the downward direction and PA = 180° to the upward direction. Also, downward electron beams are seen and highlighted with the green bar below Figure 2d.

~12:10:13, Juno crossed a boundary into the middle plasma sheet, and JADE-E observed stronger intensities of field-aligned upward going electrons with energies of the order of 2–3 keV. These beams were variable in intensity and generally of very short duration (probably <1 s; see below) as can be seen from the patterns in the energy spectrogram. JADE-E sweeps over the entire energy range in 1 s in a pyramid-like pattern. Adjacent energy steps are roughly 22% apart, and the upgoing energy steps are interleaved between the downgoing steps. Thus, if the electron beam duration is only a fraction of a second, then it is possible that the strongest intensity is measured during one of these ramps and not the other, which would explain the pattern.

After ~12:12:43 (in the inner plasma sheet), the upward beams disappeared and were replaced with a depletion of upward going electrons. We will call this an upward loss cone. Electron energies in this interval are

lower than in the previous interval, at typically a few 100 s of eV, decreasing with decreasing altitude, M shell, and/or latitude.

The southern crossing (Figure 2) was very similar to the northern one, but with some noticeable differences. This time Juno flew from low to high altitude and latitude. JADE-E measured few 100 eV electrons first (Figure 2d), with energy increasing with altitude, and then a few keV electrons. The apparent peak energy increases with altitude and latitude when Juno was connected to the inner plasma sheet was more pronounced than for the north crossing. When Juno was connected to the middle plasma sheet, the electron beam mean energies were also more variable than in the north. Similarly to the north, the low-energy electrons were depleted in the upward direction (upward loss cone, now at PA 180°) and upward electron beams appeared again in the outer plasma sheet, between ~13:29 and 13:30. The main difference between the north and the south resides in the fact that in the south, JADE-E also measured very clear downward electron beams around 13:30 and 13:32 (highlighted with the green bars below Figure 2d). After 13:32:15, Juno was in the polar region where energies increased to the point where they were beyond JADE-E's range but were still measured by JEDI [*Mauk et al*., 2017].

The red bars between Figures 1c and 1d and between Figures 2c and 2d indicate upward beam intervals, while the blue bars indicate upward loss cone intervals. The apparent depletion near PA 90° and the features that look spin modulated are the result of an artifact due to obstructions in JADE-E's field of view (FOV). During these time intervals, the magnetic field strength varied from ~1.6 to 2.1 G. In such a field, the gyroradii of electrons in JADE-E's energy range are comparable to the dimensions of spacecraft structures (~0.17 m at 100 eV and ~5.6 m at 100 keV for B = 2 G). We ran simulations of electron trajectories using a spacecraft model and assuming (1) the same energy distribution as in (Figures 1c and 2c), (2) a uniform pitch angle distribution, and (3) the magnetic field vector as reported in our data stream. The simulations' results reproduce these spin-modulated features very well. For example, they show that electrons, especially near PA 90°, are partially blocked by structures and cannot reach JADE-E's FOV, whereas near 0 or 180° PA electrons are hardly affected by these structures. The effect is more pronounced at lower energies, for which the gyroradius is the smallest. This artifact was taken into account when we derived the average PA distributions in Figure 3. We used the simulation results to account for the obstructions and corrected the rates accordingly for each energy and PA.

The colors in Figure 3 correspond to those of the intervals defined in Figures 1d and 2d top and bottom. Figures 3a and 3c show the PA distributions for the north pass and Figures 3b and 3d for the south pass for different energy ranges that are indicated in each panel. The upward direction (away from Jupiter) is on the left-hand side in all panels, which means that we have reversed the horizontal scale of Figures 3b and 3d.

We clearly see the upward beams in all panels. While there is no evidence for a downward beam in the north, it is obvious in the south (Figure 3b), although less intense than the upward beams. Also, the downward beam is only seen in the 0.1 to 4.5 keV range. Apart from the beams, the red intervals show a fairly uniform PA distribution with some small variations. These variations can be due to short times when the loss cone is visible within the beam interval, or our correction from spacecraft obstructions needs refinement, or they are just statistical variations.

In the north, the upward beam does not peak near PA = 0. This may be because the JADE-E deflection is not precisely tracking the direction of the magnetic field. JADE-E's FOV in the deflection plane is about 2–5.5°. Thus, a small difference could lead to missing the peak. The vector magnetic field received onboard is a raw value that does not yet account for offsets (e.g., due to flexing of solar panels), which can be as large as ~1°.

In Figure 3b, the downward beam from the green intervals is approximately of the same PA width as the upward beams. The downward beam is also visible from the red interval. It looks, however, more scattered (broader) in PA. Similarly to the upward beam in Figure 3a, the downward beam also does not peak at PA = 0.

Using conservation of the first adiabatic invariant, we estimate the magnetic field at the "source" of the upward electron beams assuming that the electron distribution is isotropic there and that there are no field-aligned potential drops between Juno and the source. We determine the width of the beam (in

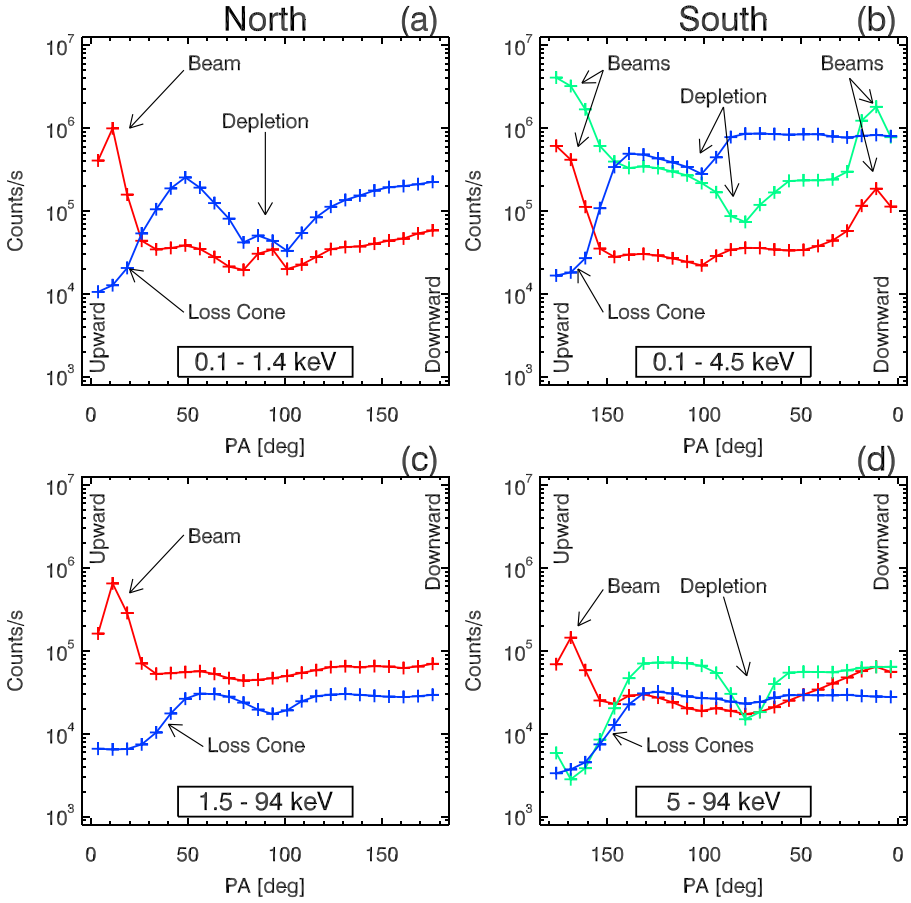

Figure 3. Pitch angle distributions for the north (a) (0.1 to 1.4 keV) and (c) (1.5 to 94 keV) and south (b) (0.1 to 4.5 keV) and (d) (5 to 94 keV) passes for the intervals defined in Figures 1 and 2 using the same colors as the bars shown in those figures. The distributions have been corrected to take into account the obstructions from spacecraft structures (see text for details). The horizontal scale of Figures 3b and 3d have been reversed so that the upward direction is on the left, as is in Figures 3a and 3c.

Figure 3) at its "base," which we define as the intersection between a line that fits the steep part of the beam (Figures 3a and 3b second to fourth data points) and a horizontal line at the average of the next three data points. We find that the beams are ~27° in the north and ~28° in the south. Using the simple relation

$$B_{\text{source}} = B_{\text{Juno}} \frac{\sin^2(\alpha_{\text{source}})}{\sin^2(\alpha_{\text{Juno}})} = \frac{B_{\text{Juno}}}{\sin^2(\alpha_{\text{Juno}})}$$

where $\alpha_{\text{source}} = 90°$, B_{Juno} and α_{Juno} are the magnetic field strength and the beam angle at Juno, respectively, we find that $B_{\text{source}} \approx 8.1$ G in the north and $B_{\text{source}} \approx 7.2$ G in the south which must place the sources very close to the surface [*Connerney et al.*, 2017a].

The PA distributions from the loss cone intervals (blue) clearly show a loss cone that is wider than the beams (~44° versus ~27° in Figure 3a and ~37° versus ~28° in Figure 3b). The decrease in intensity at the bottom of the loss cone is comparable to, but somewhat larger than, the increase in the beams. The rest of the PA distribution would be more or less uniform except for the fact that there is a depletion near PA = ~90° in the north and PA = ~80° or ~100° in the south.

The fact that the depletions hardly show in the beam intervals is evidence that they are real features. We also note that they appear during a period when the magnetic field strength changes slowly and monotonically, ruling out a possible effect due to rapidly changing magnetic field conditions. While the depletion is more or less centered on 90° in the north, it is surprising that it is near 100° (loss cone interval) or 80° (downward beam

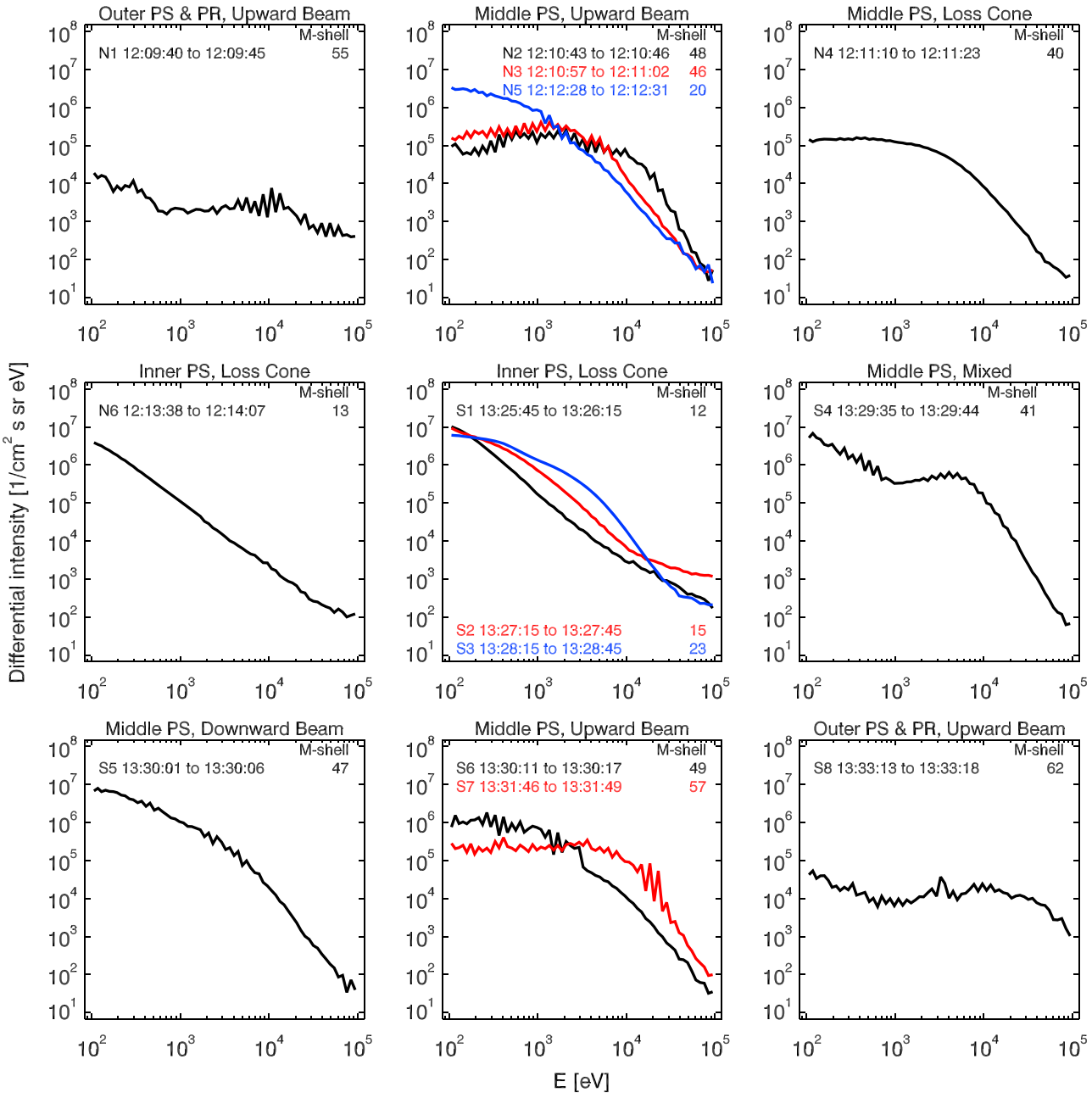

Figure 4. Electron differential intensities (averaged over look directions) as functions of energy for the intervals indicated with the black bars on top of Figures 1c and 2c. The corresponding region is indicated in the title of each panel, and the interval label and time ranges are given in the plots.

interval) in the south. We do not have any plausible explanation at this point. It is possible that despite the success of the model to reproduce the spin-modulated features in Figures 1d and 2d, the corrections applied to the PA distributions are not entirely accurate and create an apparent shift of the minimum of the depletion.

The near 90° depletion is also observed in the higher-energy electron PA distributions measured by JEDI [*Mauk et al.*, 2017, Figure 4 E5]. A potential explanation is given in *Ma et al.* [2017] where these authors report on JEDI observations of butterfly PA distributions for similar time intervals. They conclude that these particular electron distributions could be formed by parallel acceleration through Landau resonance with electrostatic waves.

The width of the loss cone (similarly defined to the beam width above) is of the order of ~44° and ~37° in the north and south, respectively. Assuming a perfect dipole, we obtain an estimate of the loss cone size by using $LC \cong \mathrm{asin}(1/R^{1.5}) \cong 30^{\circ}$. The loss cone derived from the PA distributions is somewhat bigger than our simple

estimate, perhaps due to inaccuracy in the expression, to continued scattering near Juno's location, or other causes. The width of the loss cone in the north is also larger than in the south. This could be a result of the magnetic anomaly proposed by *Grodent et al.* [2008].

Figure 4 shows differential intensities (averaged over look directions) as a function of energy for the intervals identified by the black bars above Figures 1c and 2c. Each interval is labeled with a letter ("N" for north and "S" for south) and a number which is listed in each of the nine panels with the corresponding times. Also listed is an estimate of the M shell number based on VIP4 + CAN. We picked some representative intervals in the different "regions." The sawtooth aspect of the spectra is due to beams changing faster than the duty cycle of the instrument (1 s).

The nine panels show a variety of spectral shapes with a general decrease of intensity with increasing energy. Some intervals have a peak in energy (e.g., N2, N3, and S7) within JADE-E's energy range, and others look more like tails, maybe of kappa or Maxwellian distributions, or simply like power laws (e.g., N6 and S1). Enhancements compared to a simple power law-like spectral shape are often seen (e.g., N2 to N5 and S3 to S8).

The spectra in the polar regions, or when connected to the outer plasma sheet (N1 and S8), are generally harder (flatter) than in the other regions but of much less intensity at the lower energies. There also seems to be a peak (above the typical power law-looking spectrum) near 10 keV. Although Figures 1c and 2c show rates and not differential intensities, we can still guess that this apparent peak seems to increase in energy as Juno's altitude increases. Conversely, as Juno gets closer to Jupiter and at lower latitudes, the "peak" (or enhancement) decreases to a few keV (N2 to N5 and S3 to S7) until it is no longer visible in this energy range (N6 and S1). The enhancements in the spectra when connected to the middle plasma sheet typically occur between 1 and 10 keV. When connected to the inner plasma sheet, the enhancement only appears occasionally below 1 keV (S2 and S3). The spectrum for interval S4 represents a mixture of both a loss cone feature and downward beam, which may explain its peculiar shape.

4. Conclusions

JADE-E measured 0.1–100 keV electrons for the first time at low altitude in the auroral regions of Jupiter. This study focuses on when Juno was flying over the regions connected to near the main auroral oval and JADE was collecting high time resolution (1 s) PA and energy distributions.

Looking at Figures 1c, 1d, 2c, and 2d, the structures observed by JADE-E are similar between the north and the south pass and look somewhat mirrored in time. The electron energy decreases with decreasing latitude. It is highest (tens of keV or higher) when connected to the outer magnetosphere/polar regions and lowest (tenths of keV or lower) when connected to the inner plasma sheet (region connected near to the main auroral oval). Amongst the most remarkable features of this first science orbit, JADE-E observed upward and downward electron beams. Note that upward electron beams were also seen at Earth [*Carlson et al.*, 1998] and Saturn [*Saur et al.*, 2006, *Mitchell et al.*, 2009]. Also, a recent model by *Ozak et al.* [2013] gives examples of secondary electron fluxes escaping from Jupiter's upper atmosphere caused by ion precipitation. JADE and JEDI's measurements could be used to provide constraints to their model and to adjust upward electron fluxes.

The downward electron beams were only seen in the south near the transition between the inner and middle plasma sheet. Thus, we see little evidence of strongly accelerated downward electrons analogous to the auroral "inverted Vs" at Earth.

JADE-E also identified upward loss cones at ~66 to 69° latitude in the north (~1.55 to 1.62 R_J) and ~62 to 66° in the south (~1.54 to 1.63 R_J), when it was connected to the inner plasma sheet. These structures suggest a diffuse aurora process [see *Mauk et al.*, 2017]. Particles are trapped on the field lines with a reasonably isotropic distribution outside of the loss cones. However, the scattering of the particles, presumably by wave-particle interactions, fills the loss cones. At low altitudes, then, the downward loss cones are full. But those downward particles strike the upper atmosphere and are lost, and so the upward loss cone is empty.

Often, when Juno is connected to the middle plasma sheet, rapid changes, on a timescale shorter than the 1 s duty cycle of JADE-E, are seen in the energy spectra (sawtooth patterns in Figure 4). These rapid changes suggest that the auroral structures have very fine spatial scales on the order of a few tens of kilometers (Juno's

speed is ~45–48 km/s for the intervals presented here). Some of these structures are associated with sources of electron cyclotron maser instabilities [*Louarn et al*., 2017, *Kurth et al*., 2017].

In summary, JADE-E identified electron beams, mostly upward going but also some downward going in the south, above the auroral regions at latitudes from ~69 to 72° and ~ −66° to −70° corresponding to M shells from ~18 to 54 and ~28 to 61, respectively. At somewhat lower latitudes, the beams were replaced by upward loss cones, suggestive of a diffuse auroral process. The energy spectra resemble tails of distributions or power laws (suggestive of a stochastic acceleration process) but can also have some clear enhancements or even peaks generally between 1 and 10 keV. Electron intensity changes on timescales of a second or less indicate that auroral structures can be of the order of a few tens of kilometers.

These first passes over the auroral regions of Jupiter have already revealed unprecedented plasma measurements. Future studies will include correlations of in situ plasma measurements with optical features (e.g., *Bonfond et al*. [2017]), energetic particle measurements, radio waves (e.g., *Louis et al*. [2017]), and magnetic field measurements.

Acknowledgments
We thank all the outstanding women and men who have made JADE and Juno a reality. This work was funded by the NASA New Frontiers Program for Juno. The data presented here—The JNO-J/SW-JAD-3-CALIBRATED-V1.0 and JNO-J/SW-JAD-2-UNCALIBRATED-V1.0—will reside at NASA's Planetary Data System (http://pds.nasa.gov/, March 2017). It now resides at the Laboratory for Atmospheric and Space Physics at the University of Colorado Boulder. That site is password controlled, but access for evaluation can be obtained by contacting the lead author of this paper.

References

Adriani, A., et al. (2014), JIRAM, the Jovian Infrared Auroral 270 Mapper, *Space Sci. Rev.*, 1–54, doi:10.1007/s11214-014-0094-y.
Bagenal, F., et al. (2014), Magnetospheric science objectives of the Juno mission, *Space Sci. Rev.*, 1–69, doi:10.1007/s11214-014-0036-8.
Bonfond, B., D. Grodent, J.-C. Gérard, T. Stallard, J. T. Clarke, M. Yoneda, A. Radioti, and J. Gustin (2012), Auroral evidence of Io's control over the magnetosphere of Jupiter, *Geophys. Res. Lett.*, *39*, L01105, doi:10.1029/2011GL050253.
Bonfond, B., et al. (2017), Morphology of the UV aurorae Jupiter during Juno's first perijove observations, *Geophys. Res. Lett.*, *44*, 4463–4471, doi:10.1002/2017GL073114.
Carlson, C. W., et al. (1998), FAST observations in the downward auroral current region: Energetic upgoing electron beams, parallel potential drops, and ion heating, *Geophys. Res. Lett.*, *25*, 2017–2020, doi:10.1029/98GL00851.
Connerney, J. E. P., M. H. Acuna, and N. F. Ness (1981), Modeling the Jovian current sheet and inner magnetosphere, *J. Geophys. Res.*, *86*, 8370–8384, doi:10.1029/JA086iA10p08370.
Connerney, J. E. P., M. H. Acuna, N. F. Ness, and T. Satoh (1998), New models of Jupiter's magnetic field constrained by the Io flux tube footprint, *J. Geophys. Res.*, *103*, 11929–11940, doi:10.1029/97JA03726.
Connerney, J. E. P., et al. (2017a), Jupiter's Magnetosphere and Aurorae Observed by the Juno Spacecraft During its First Polar Orbits, *Science*, doi:10.1126/science.aam5928.
Connerney, J. E. P., et al. (2017b), The Juno Magnetic Field Investigation, *Space Sci. Rev.*, doi:10.1007/s11214-017-0334-z.
Ebert, R. W., et al. (2017), Accelerated Flows at Jupiter's Magnetopause: Evidence for Magnetic Reconnection Along the Dawn Flank, *Geophys. Res. Lett.*, *44*, 4401–4409, doi:10.1002/2016GL072187.
Gershman, D. J., et al. (2017), Juno observations of large-scale compressions of Jupiter's dawnside magnetopause, *Geophys. Res. Lett.*, doi:10.1002/2017GL073132, in press.
Gladstone, G. R., et al. (2014), The ultraviolet spectrograph on NASA's Juno mission, *Space Sci. Rev.*, 1–27, doi:10.1007/s11214-014-0040-z.
Grodent, D., B. Bonfond, J.-C. Gérard, A. Radioti, J. Gustin, J. T. Clarke, J. Nichols, and J. E. P. Connerney (2008), Auroral evidence of a localized magnetic anomaly in Jupiter's northern hemisphere, *J. Geophys. Res.*, *113*, A09201, doi:10.1029/2008JA013185.
Kurth, W., et al. (2017), A New View of Jupiter's Auroral Radio Spectrum, *Geophys. Res. Lett.*, *44*, doi:10.1002/2017GL072889.
Louis, C. K., et al. (2017), Io-Jupiter decametric arcs observed by Juno/Waves compared to ExPRES simulations, *Geophys. Res. Lett.*, *44*, doi:10.1002/2017GL073036.
Louarn, P., et al. (2017), Generation of the Jovian hectometric radiation: First lessons from Juno, *Geophys. Res. Lett.*, *44*, 4439–4446, doi:10.1002/2017GL072923.
Ma, Q., et al. (2017), Electron butterfly distributions at particular magnetic, *Geophys. Res. Lett.*, *44*, 4489–4496, doi:10.1002/2017GL072983.
Mauk, B. H., et al. (2014), The Jupiter Energetic Particle Detector Instrument (JEDI) investigation for the Juno mission, *Space Sci. Rev.*, 1–58, doi:10.1007/s11214-013-0025-3.
Mauk, B. H., et al. (2017), Juno observations of energetic charged particles over Jupiter's polar regions: Analysis of mono-and bi-directional electron beams, *Geophys. Res. Lett.*, *44*, 4410–4418, doi:10.1002/2016GL072286.
McComas, D. J., et al. (2013), The Jovian Auroral Distributions Experiment (JADE) on the Juno mission to Jupiter, *Space Sci. Rev.*, 1–97, doi:10.1007/s11214-013-9990-9.
McComas, D. J., et al. (2017), Plasma environment at the dawn flank of Jupiter's magnetosphere: Juno arrives at Jupiter, *Geophys. Res. Lett.*, *44*, 4432–4438, doi:10.1002/2017GL072831.
Mitchell, D. G., W. S. Kurth, G. B. Hospodarsky, N. Krupp, J. Saur, B. H. Mauk, J. F. Carbary, S. M. Krimigis, M. K. Dougherty, and D. C. Hamilton (2009), Ion conics and electron beams associated with auroral processes on Saturn, *J. Geophys. Res.*, *114*, A02212, doi:10.1029/2008JA013621.
Ozak, N., T. E. Cravens, and D. R. Schultz (2013), Auroral ion precipitation at Jupiter: Predictions for Juno, *Geophys. Res. Lett.*, *40*, 4144–4148, doi:10.1002/grl.50812.
Phillips, J. L., S. J. Bame, B. L. Barraclough, D. J. McComas, R. J. Forsyth, P. Canu, and P. J. Kellogg (1993), Ulysses plasma electron observations in the Jovian magnetosphere, *Planet. Space Sci.*, *41*(11–12), 877–892, doi:10.1016/0032-0633(93)90095-J.
Radioti, A., A. T. Tomás, D. Grodent, J.-C. Gérard, J. Gustin, B. Bonfond, N. Krupp, J. Woch, and J. D. Menietti (2009), Correction to "Equatorward diffuse auroral emissions at Jupiter: Simultaneous HST and Galileo observations", *Geophys. Res. Lett.*, *36*, L09103, doi:10.1029/2009GL038676.
Saur, J., et al. (2006), Anti-planetward auroral electron beams at Saturn, *Nature*, *439*, 699–702, doi:10.1038/nature04401.
Szalay, J. R., et al. (2017), Plasma measurements in the Jovian polar region with Juno/JADE, *Geophys. Res. Lett.*, doi:10.1002/2017GL072837.
Valek, P. W., et al. (2017), Hot Flow Anomaly Observed at Jupiter's Bow Shock, *Geophys. Res. Lett.*, *44*, doi:10.1002/2017GL073175.
Vogt, M. F., M. G. Kivelson, K. K. Khurana, R. J. Walker, B. Bonfond, D. Grodent, and A. Radioti (2011), Improved mapping of Jupiter's auroral features to magnetospheric sources, *J. Geophys. Res.*, *116*, A03220, doi:10.1029/2010JA016148.